Opto-Electronic Advances

Supplementary information

2021, Vol. 4, No. 11

DOI: 10.29026/oea.2021.210002

Near-perfect fidelity polarization-encoded multilayer optical data storage based on aligned gold nanorods

Linwei Zhu[1†], Yaoyu Cao[2†], Qiuqun Chen[3], Xu Ouyang[2], Yi Xu[2], Zhongliang Hu[3], Jianrong Qiu[3,4*] and Xiangping Li[2*]

[1]School of Physics and Optoelectronic Engineering, Ludong University, Yantai 264025, China; [2]Guangdong Provincial Key Laboratory of Optical Fiber Sensing and Communications, Institute of Photonics Technology, Jinan University, Guangzhou 510632, China; [3]State Key Laboratory of Luminescent Materials and Devices, and Institute of Optical Communication Materials, South China University of Technology, Guangzhou 510640, China; [4]State Key Laboratory of Modern Optical Instrumentation, College of Optical Science and Engineering, Zhejiang University, Hangzhou 310027, China.

[†]These authors contributed equally to this work.

[*]Correspondence: JR Qiu, E-mail: qjr@scut.edu.cn; XP Li, E-mail: xiangpingli@jnu.edu.cn

This file includes:

Supplementary information for this paper is available at https://doi.org/10.29026/oea.2021.210002

Section 1: Preparation of the nanocomposite film involving aligned GNRs

A. Preparation of the GNRs solution using two steps seed-mediated growth method

GNRs can be produced utilizing the seed-mediated growth method reported by Murray et al[1,2]. The flow diagram for the preparation of GNRs is shown in Fig. S1.

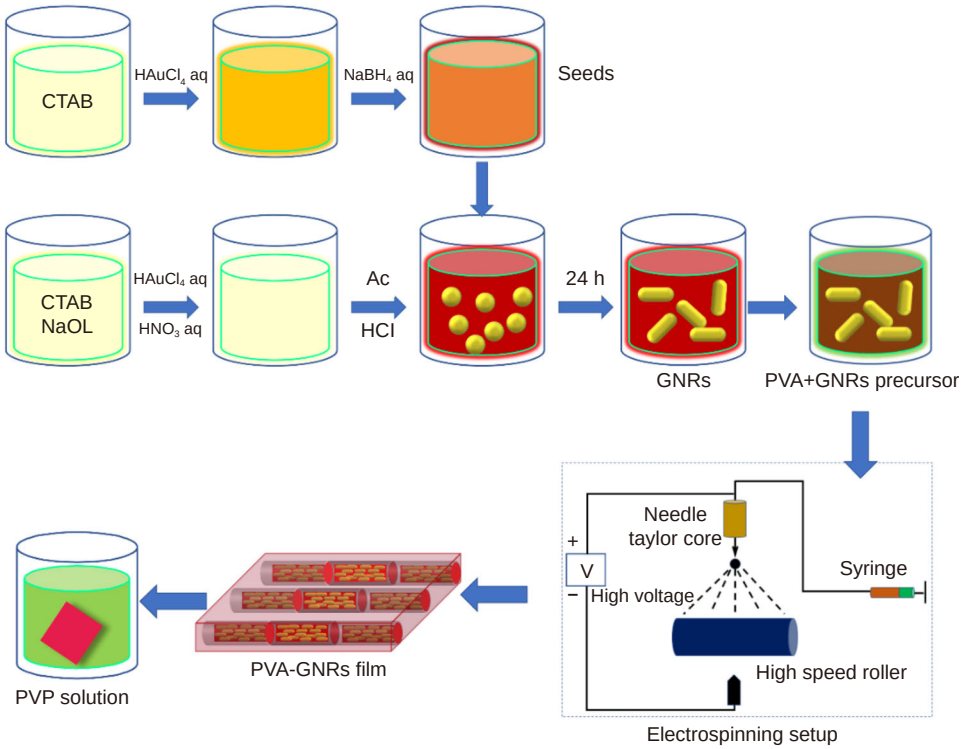

Fig. S1 | The schematic diagram for preparing the nanocomposite film with aligned gold nanorods

Step 1, Preparing the seed solution:

1) Prepare CTAB (Cetyltrimethyl Ammonium Bromide, 0.1 M, 9.5 mL) solution with transparent color.

2) Add an aqueous solution $HAuCl_4$ (0.01 M, 0.25 mL) into CTAB solution, and stir intensely to orange-yellow color.

3) Add freshly ice-cold $NaBH_4$ (0.01 M, 0.6 mL) aqueous solution into the mixture consisting of $HAuCl_4$ and CTAB, stirr quickly for two minutes to turn brown color, and then leave it undisturbed for 30 minutes. The first step to produce the seed solution is finished.

Step 2, Growing of the GNRs:

1) Put CTAB (6.15 g) and NaOL (1.543 g) into Milli-Q water (250 mL) until completely dissolved.

2) Add $AgNO_3$ (4 mM, 12 mL) aqueous solution and stir for 15 minutes, then add $HAuCl_4$ (1 mM, 250 mL) aqueous solution and stir for 150 minutes, then wait for the solution to change from yellow to colorless.

3) Add HCl (1.0 M, 4 mL) solution, after 15 minutes add ascorbic acid (0.064 M, 1.25 mL) solution, and conduct gentle mixing for 30 seconds.

4) Finally, add the seed solution (1.6 mL) to the growth solution, stir intensely for 30 seconds, and leave it undisturbed for at least 12 h. The GNRs solution is finished.

The GNRs with various average aspect ratios can be produced by controlling the concentration of the HAuCl4, the amount of seed solution, and the growth temperature.

B. Preparation of the precursor solution with fully dispersed GNRs for electrospinning

First, purify the prepared GNRs solution to remove excess CTAB by centrifugation (10000 rpm for 10 min). Second, prepare 13 wt % PVA (polyvinyl alcohol) aqueous solution by putting PVA (2.6 g) into Milli-Q water (17.4 mL) and stirring for 2 hours. Third, add the concentrated GNRs (100 mM, 0.6 mL) into 13 wt % PVA (2.4 mL) aqueous solution

under vigorous stirring to fully disperse GNRs. Finally, the 8 wt % precursor solution consisting of fully dispersed GNRs and PVA is prepared, left undisturbed at least 12 hours for standby.

C. Preparation of the PVA nanofibers with aligned GNRs

The PVA nanofibers with aligned GNRs can be produced by an electrospinning setup, as shown in Fig. S1. First, load the precursor solution consisting of homogeneous GNRs into a 20 mL plastic syringe. Then the precursor solution is pumped to the needle at a flow rate of 1.0 mL/h. During electrospinning: a high voltage of 10.0 kV is applied to the needle. A high-speed roller with a rotating speed of 3000 rpm is driven by a motor with a high voltage of −8 kV, which is used to collect the electrospun nanofibers involving aligned GNRs.

D. Preparation of the transparent composite film

In order to eliminate or induce serious scattering resulted from the mismatch of the refraction index between the air and the PVA nanofibers, another material with a refractive index similar to PVA is selected to fill in space between PVA fibers, which makes the composite film transparent. In detail, the tailored composite film is soaked into 0.05 g/mL PVP (polyvinyl pyrrolidone, $M_w \approx 1300000$, $n = 1.51$) alcoholic solution and pulled-out. The step is repeated three times every 10 minutes. Then, the PVP solution containing the PVA films is shifted into an oven and baked at 50 °C until the solution is thoroughly dried.

Section 2: Characterization of the nanocomposite film

In the experiment, we prepared nanocomposite films involving the aligned GNRs with different average aspect ratios (AR = 3.4 and 4.8), named PVA-GNRs-3.4-PVP and PVA-GNRs-4.8-PVP. Figure S2(a) and S2(b) show images of the nanocomposite films and the corresponding SEM and TEM images involving GNRs with different average AR of 3.4 and 4.8, respectively. From the digital photos of the composite films, we can see that the composite films involving GNRs of different AR have different colors. We can also see that the collected PVA nanofibers exhibited a very high degree of alignment, as shown in SEM images. Moreover, as shown in the TEM images, the axis of the longitudinal axis of GNRs is parallel to the aligned axis of PVA nanofibers. The experimental results show that a large area of composite film with highly oriented GNRs can be prepared.

Figure S2(c) shows the normalized absorption spectra of the GNRs with different aspect ratios (AR=3.4, 4.8) in the water environment, recorded with a Perkin Elmer Lambda 900 UV−vis-IR spectrometer. We can see that each sample has two absorption peaks, which are attributed to the absorptions of longitudinal localized surface plasmon resonance (LSPR) and transversal localized surface plasmon resonance (TSPR) mode, respectively. One is located at 520 nm, which is the TSPR absorption peak of the GNRs, and it does not change with the AR of the GNRs. The other is the LSPR absorption peak of the GNRs, which shifts to longer wavelengths with increasing aspect ratios of the GNRs. The LSPR absorption peaks of the GNRs with AR=3.4 and AR=4.8 are located at 750 nm and 895 nm, respectively. The normalized absorption spectra of the prepared composite films (PVA-GNRs-PVP) GNRs are shown in Fig. S2(d). The LSPR absorption peak of the composite films is located at approximately 800nm and 955nm, about 50 nm-redshift compared to the original GNRs, which can be attributed to the increase of dielectric constant around GNRs in the composite film.

Figure S2(e) and S2(f) show the polarized absorption spectra of the composite films with different aspect ratios of aligned GNRs. When the orientation of the nanofiber is parallel to the polarization orientation of the incident light, the TSPR mode of the GNRs cannot be excited, while the LSPR mode of the GNRs can be excited. As shown in the Fig. S2(e) and S2(f), the LSPR absorption peak is large, while the TSPR absorption peak is small. When the orientation of the nanofiber is perpendicular to the polarization orientation of the incident light, the LSPR mode of the GNRs is difficult to be excited, while the TSPR mode of the GNRs can be excited. So, we can see a significant increase in the TSPR absorption peak and a decrease in the LSPR absorption peak.

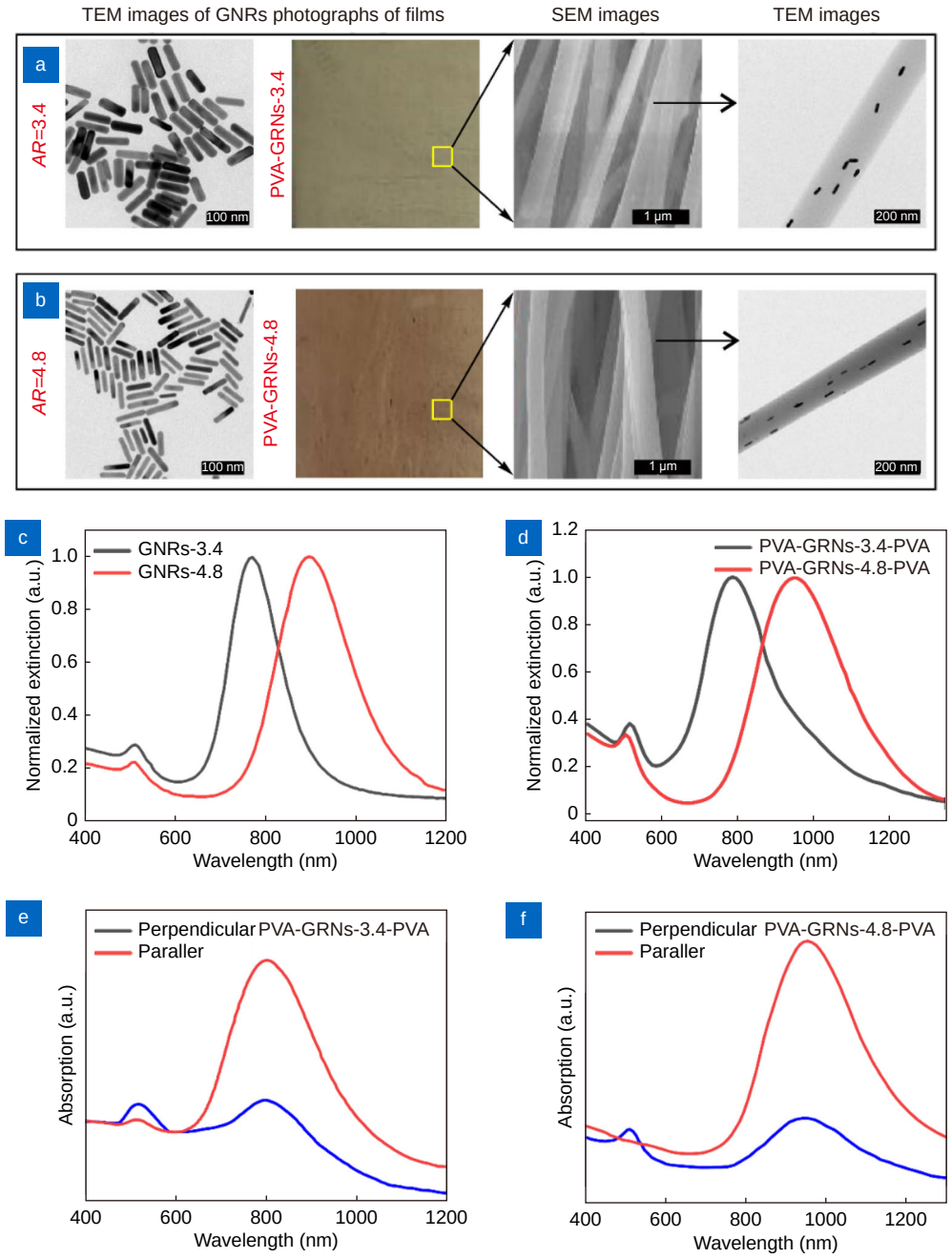

Fig. S2 | Images of the nanocomposite films and the corresponding SEM and TEM images involving GNRs with different average AR of (**a**) 3.4 and (**b**) 4.8. (**c**) Absorption spectra of GNRs in aqueous solution. (**d**) Extinction spectra of PVA-GNRs-PVP composite film. (**e**) and (**f**) Polarized absorption spectra of the composite films.

Section 3: Polarization property of the TPL intensity distribution of the sample

It is known that the TPL intensity reaches the maximum when the polarization of the excitation light is parallel to the long axis of GNRs. This polarization characteristic of the TPL intensity can be used to determine the orientation of the aligned GNRs contained in the composite films. Figure S3(a) shows typical TPL intensity distributions for the composite film with aligned GNRs of aspect ratio 3.4. The composite film was excited by the femtosecond laser (800 nm, 140 fs, 80 MHz). The TPL intensity images are recorded by the APD (scanning area 40 μm × 40 μm). The polarization orientation of the excitation light is tuned by rotating the half-wave plate. Figure S3(b) shows the TPL signal as a function of the orientation angle. In Fig. S3(b), the TPL signal is calculated by summing the TPL intensity of the whole scanning area. We can see that the TPL signal meets a $\cos^4(\theta-\varphi)$ dependence (φ is the orientation angle of the long axis of the

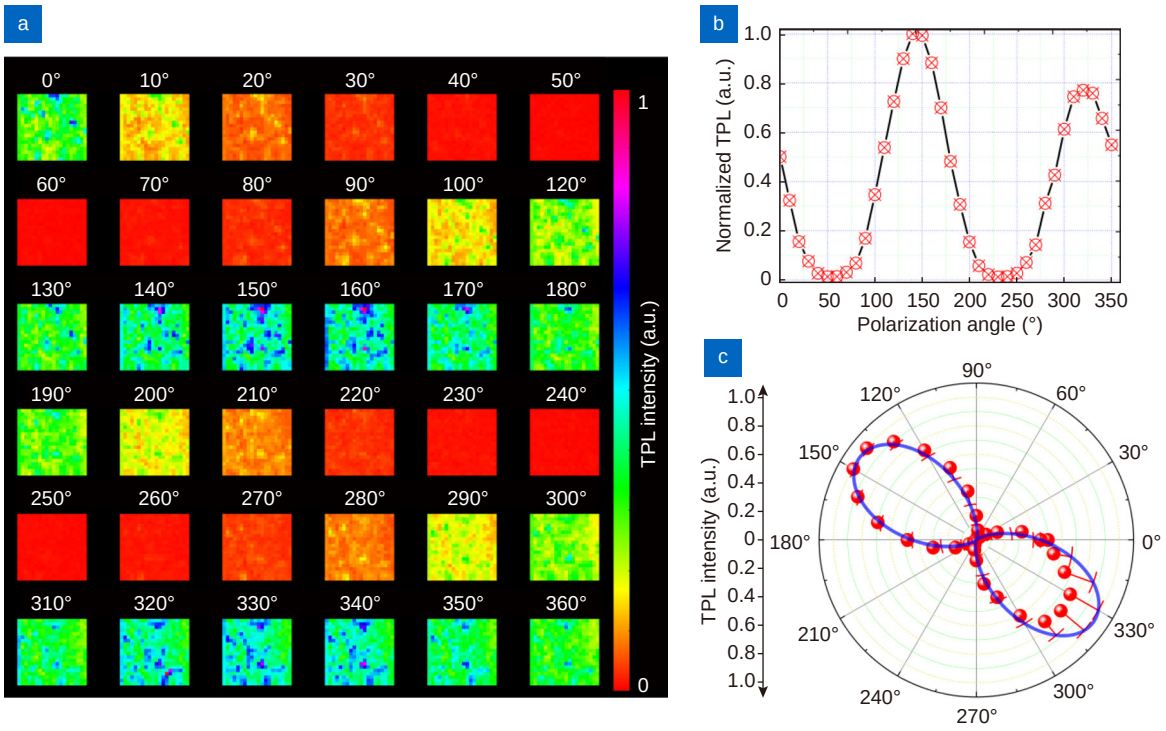

Fig. S3 | (**a**) TPL intensity distribution with different polarization angles. (**b**) TPL polarization sensitivity of the sample excited by the 800 nm femtosecond laser. (**c**) Shows the polar plots of the TPL intensity. The blue curves are plotted according to the best-fitted biquadratic cosine function.

aligned GNRs. θ is the polarization angle of the light). Figure S3(c) shows the polar plot of the TPL signal. The experimental resulted is in good agreement with the theory, which further illuminates that the composite film possesses a high degree of alignment GNRs. Therefore, based on the polarization characteristic of the TPL signal, we can determine the alignment angles of the GNRs.

Section 4: The fidelity defined by the correlation coefficient and bit error rate

In this paper, the correlation coefficient is applied to characterize the fidelity of pattern data extracted by recording the two-photon-induced luminescence (TPL) intensities of all the information units. Figure S4(a) shows the original pattern for recording. Figure S4(b) shows the extracted pattern of the TPL intensity. The statistical histogram (blue color) of the TPL intensity of all the information units is shown in Fig. S4(d). We can see two Gaussian distributions with different average intensities, corresponding to the information units without and with the irradiation of femtosecond laser pulses, respectively. A threshold intensity $I_{\rm th}$ is used to discriminate the two types of information units and to apply binarization. The correlation coefficient can be deduced after the binarization of the extracted pattern. As shown in Fig. 4S(c), the binarized pattern is changing with different $I_{\rm th}$. The red units denote the error information units compared to the original data after binarizing the extracted pattern. The extracted pattern can be binarized by choosing an appropriate threshold intensity to obtain a maximum correlation coefficient.

The correlation coefficient between the binarized pattern and the original one is defined as follows:

$$c = \frac{\sum_m \sum_n (A_{mn} - \bar{A})(B_{mn} - \bar{B})}{\sqrt{\left[\sum_m \sum_n (A_{mn} - \bar{A})^2\right]\left[\sum_m \sum_n (B_{mn} - \bar{B})^2\right]}}, \tag{S1}$$

where $\bar{A} = \Sigma_m \Sigma_n A_{mn}/(mn)$, $\bar{B} = \Sigma_m \Sigma_n B_{mn}/(mn)$. Here, A_{mn} and B_{mn} represent the intensities of individual pixel-units (m, n) while $\bar{A}$ and $\bar{B}$ denote the averaged intensities of all the pixels in the binarized readout pattern and original patterns, respectively. The correlation coefficient as a function of the threshold intensity $I_{\rm th}$ is shown in Fig. 4S(d). We can see that a maximum correlation coefficient of c = 0.997 is obtained by Eq. (S1) when the threshold intensity $I_{\rm th}$ = 0.37 is se-

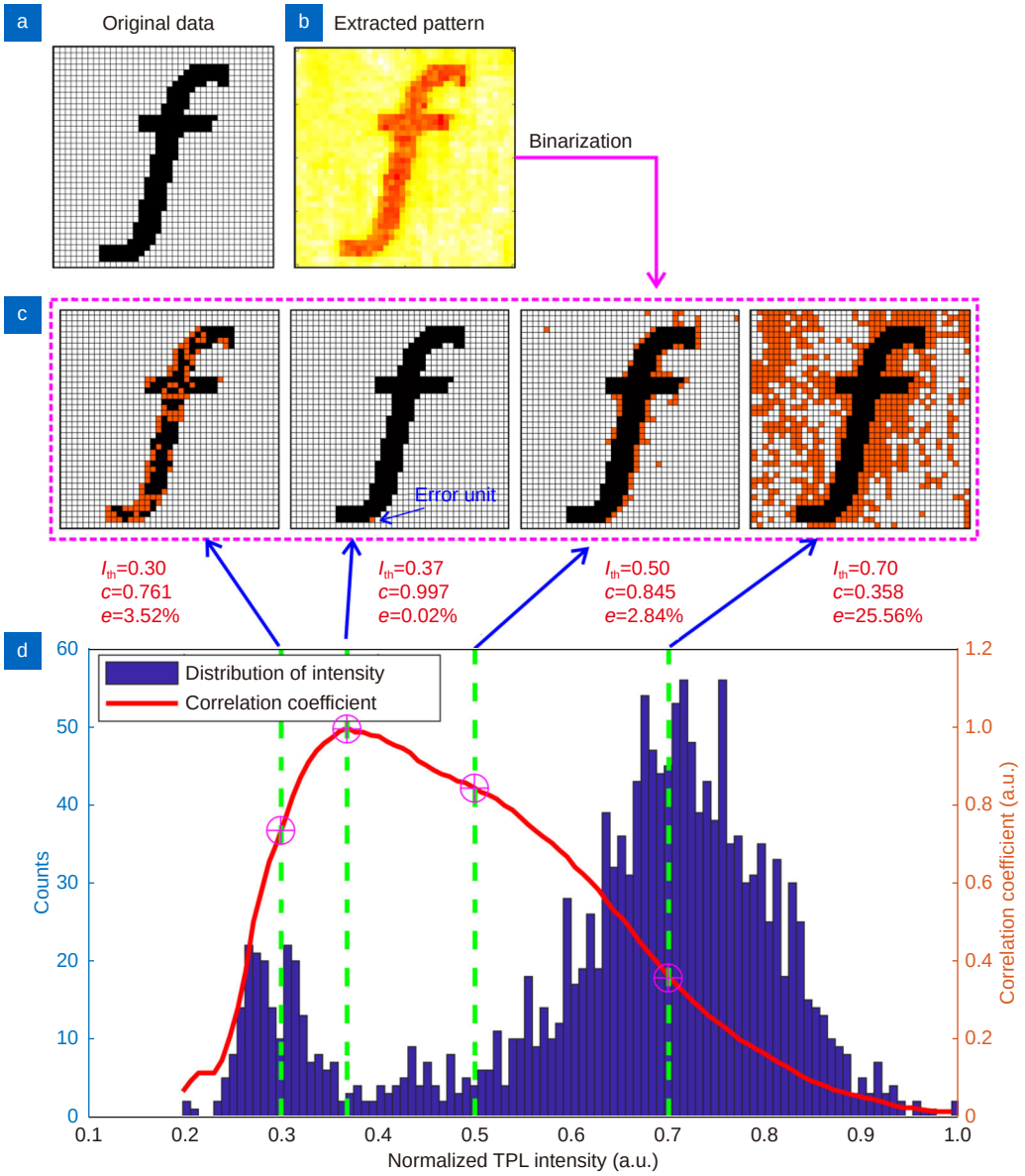

Fig. S4 | Procedure used to derive the correlation coefficient and bit error rate of an extracted pattern. (**a**) The original pattern used for data recording. (**b**) The pattern obtained by detecting the TPL intensities of all the information units. (**c**) The binarized patterns obtained by choosing various threshold intensities. Here, the red units denote the error of the information units between the original data and the extracted binarization data. The calculated correlation coefficients and bit error rates for the extracted pattern with different threshold intensity I_{th} are also provided. (**d**) The statistical histogram distribution (blue) and the correlation coefficient curve depending on the normalized TPL intensities of all the information units in the extracted pattern.

lected to binarize the extracted pattern. Another parameter that characterizes the quality of the extracted pattern is bit error rate (BER), which is defined as:

$$e = \frac{\sum_m \sum_n |A_{mn} - B_{mn}|}{N} . \tag{S2}$$

Here, $|A_{mn} - B_{mn}|$ denotes the error bit between the original data and the extracted binarization data of all the information units. N is the total number of information units. As shown in Fig. S4(c), when the threshold intensity I_{th} = 0.37, there is only one error bit of the extracted binarization pattern compared with the original pattern. The bit error rate is e=0.02% calculated by Eq. (S2). These results show that the highly aligned GNRs inside of the composite film enables the recording and reading of information with high encoding/decoding fidelity and low bit error rate.

Section 5: The two-layers ODS using aligned GNRs

Figure S5 shows the experimental results of the two-layers ODS using two composite films, in which the orientations of the nanofibers are different. Figure S5(a) shows the two patterns for writing in the ODS media with two layers of the composite films. The readout patterns of the TPL intensity are shown in Fig. S5(b). The corresponding statistical histograms of the TPL intensities of all the pixels are shown in Fig. S5(d) and S5(e), respectively. By opting for suitable thresholds of the normalized TPL, the information units can be recovered from binarized processing. Figure S5(c) shows the optimal binarized pattern. The correlation coefficient can be calculated after the binarization of the readout pattern. We can see that multilayers ODS with high-fidelity (c > 99%) have been achieved by selecting suitable thresholds for the normalized TPL. As can be seen from these results, the crosstalk between different layers is small, and the bit error rates are also very low ($e \approx 0.1\%$), validating the possibility to realize polarization-encoded multilayers ODS with near-perfect fidelity utilizing the materials of the aligned GNRS.

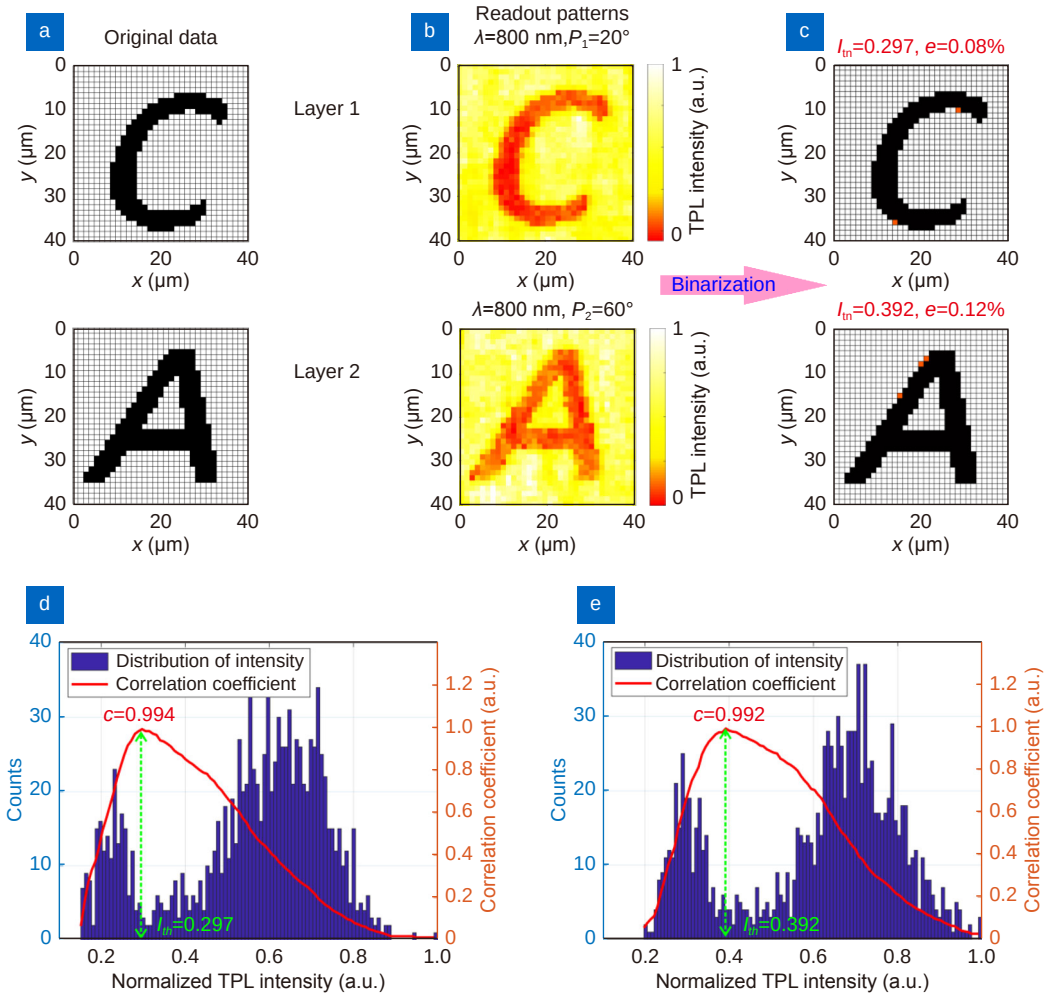

Fig. S5 | (**a**) The original patterns for recording in the two layers inside of aligned GNRs. (**b**) The retrieved results for the two types of combination with different layers and polarizations. (**c**) The binarization patterns at the optimal threshold intensities. (**d**) and (**e**) The statistical charts of the TPL intensities detected from all information units in (b). The calculated correlation coefficients for the extracted pattern are also provided.

Section 6: The two-layers ODS using randomly aligned GNRs

In order to compare the fidelity of the ODS with the composite films of the aligned GNRS, we performed the ODS experiment using the storage medium of randomly aligned GNRs. For this purpose, a storage medium composed of randomly aligned GNRs is fabricated by using the same method presented in refs.[3]. The original data encoded in different layers are shown in Fig. S6(a). The recording area is 40 μm × 40 μm in size (50 × 50 pixels). They are recorded with the same wavelength and while utilizing different polarization (P_1 = 0°, P_2 = 40°), respectively. The recording and readout

power are 500 μW and 150 μW, respectively. Such encoded information can be read out by the laser with the same polarization and wavelength in the recording. Figure S6(b) shows the readout patterns of the TPL intensity distributions in two layers. Figure 6S(d) and 6S(e) show the corresponding statistical results of TPL intensity collected in each pixel of Fig. S6(b), respectively. We can see that the correlation coefficients vary with different layers. The correlation coefficient (c = 0.794) in the bottom layer is small because of the crosstalk induced by the upper layer. Moreover, the fidelity of data in the ODS medium with randomly aligned GNRs is smaller than that in the material of aligned GRNs. As shown in Fig. S6(c), the bit error rates (e = 1.89%, e = 5.78%) readout from randomly aligned GNRs are more than ten times higher than that from aligned GNRs (shown in Fig. S5).

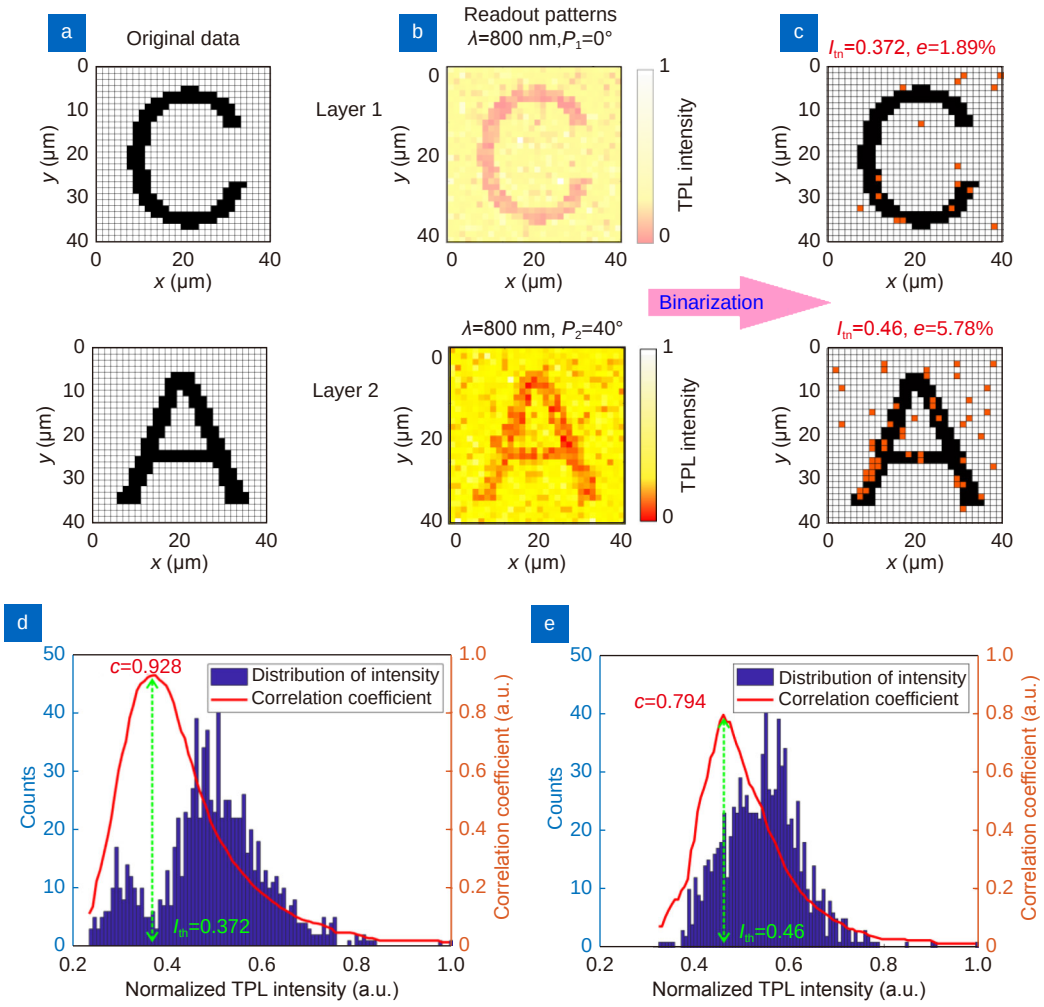

Fig. S6 | (**a**) The original patterns for recording in the two layers inside of randomly aligned GNRs. (**b**) The retrieved results for the two types of combination with different layers and polarizations. Here, the corresponding wavelength and polarization are shown in the figures. (**c**) The binarization patterns at the optimal threshold intensities. (**d**) and (**e**) The statistical charts of the TPL intensities detected from all information units in (b). The calculated correlation coefficients for the extracted pattern are also provided.

Section 7: The transmission through the multilayers with aligned GNRs and randomly aligned GNRs

In general, increasing the number of layers used in optical data storage media can effectively increase the storage capacity but can also have heavy optical losses for deep layers. However, compared with the randomly aligned GNRs for polarization-encoded multilayered ODS, the prepared nanocomposite film involving aligned GNRs will be highly beneficial in reducing optical losses. An exemplifying situation for the signal loss in a simple multilayer setting can be seen by plotting the ratio of readout signal power with respect to input power. Assuming that the recording medium consists of GNRs with uniform size and aspect ratio, the governing equation for the ratio of TPL signal power to the input laser power can be written as[4]:

$$\xi(\theta, m) = \frac{NA^2}{\pi(0.61\lambda)^2}\eta\sigma_{ab}\cos^4(\phi_m - \theta_{pol})\, t(\theta, m) \ , \tag{S3}$$

where η is the luminescence quantum yield, and σ_{ab} is the TPA cross-section of GNRs at the SPR peak. The term $\cos^4(\theta_{pol}-\phi_m)$ accounts for the sequential twisting of GNRs alignment for the m layer. $t(\theta, m)$ is the transmission through the multilayers, which is given by[5]

$$t(\theta, m) = \prod_{i=1}^{m}\left[\exp\left(-\alpha_{ext} - \delta\right)\right] , \tag{S4}$$

where m is the number of the layers. δ is the residual absorbance of the space layer. α_{ext} is the polarization-dependent extinction coefficient, which gives the total extinction cross-sections of summing the corresponding extinction cross-sections of the GNRs in each distribution. The extinction coefficient α_{ext} can be expressed as

$$\alpha_{ext} = \sum_{k=1}^{n}\sigma_{ext}\cos^2\left(\phi_k - \theta_{pol}\right)N/n. \tag{S5}$$

Here the summation is over the n GNRs within the simulated ensemble. N is the areal number density of the GNRs in a single layer, σ_{ext} is the extinction cross-section, ϕ_k is the orientation angle of each nanorod in the ensemble n, and θ_{pol} is the polarization angle of the light.

Figure S7(a) shows an exemplifying drawing of a multilayer structure with aligned GNRs and Fig. S7(b) shows the corresponding plots of polarization-dependent transmission calculated by Eq. (S3–S5), for a ten-layer structure with areal density of $N = 2.4 \times 10^{13}$ m^{-2} and residual absorbance $\delta = 0$. The other simulated parameters are: the extinction cross-section $\sigma_{ext} = 3.04 \times 10^{-14}$, NA=1.4, λ=800 nm. Figure S7(c) and S7(b) show examples of a multilayer structure with randomly aligned GNRs and its corresponding plots of polarization-dependent transmission. Figure S7(e) shows the comparison curves of transmission between the aligned and randomly aligned GNRs throughout the layers at the optimum polarization of excitation light. One can see a great improvement in the transmission of aligned GNRs at all layers. Therefore, this property of polarization-encoded TPL readout in progressively twisted aligned GNRs arrays through the multilayers to make it possible through deeper layers without too much extinction loss. We have shown that rotating the alignment angle of the GNRs between each layer, together with the polarization-encoded for readout, can further reduce the loss in multilayer ODS and simultaneously maintain near-perfect fidelity for encoding information, which is previously impossible with random GNRs.

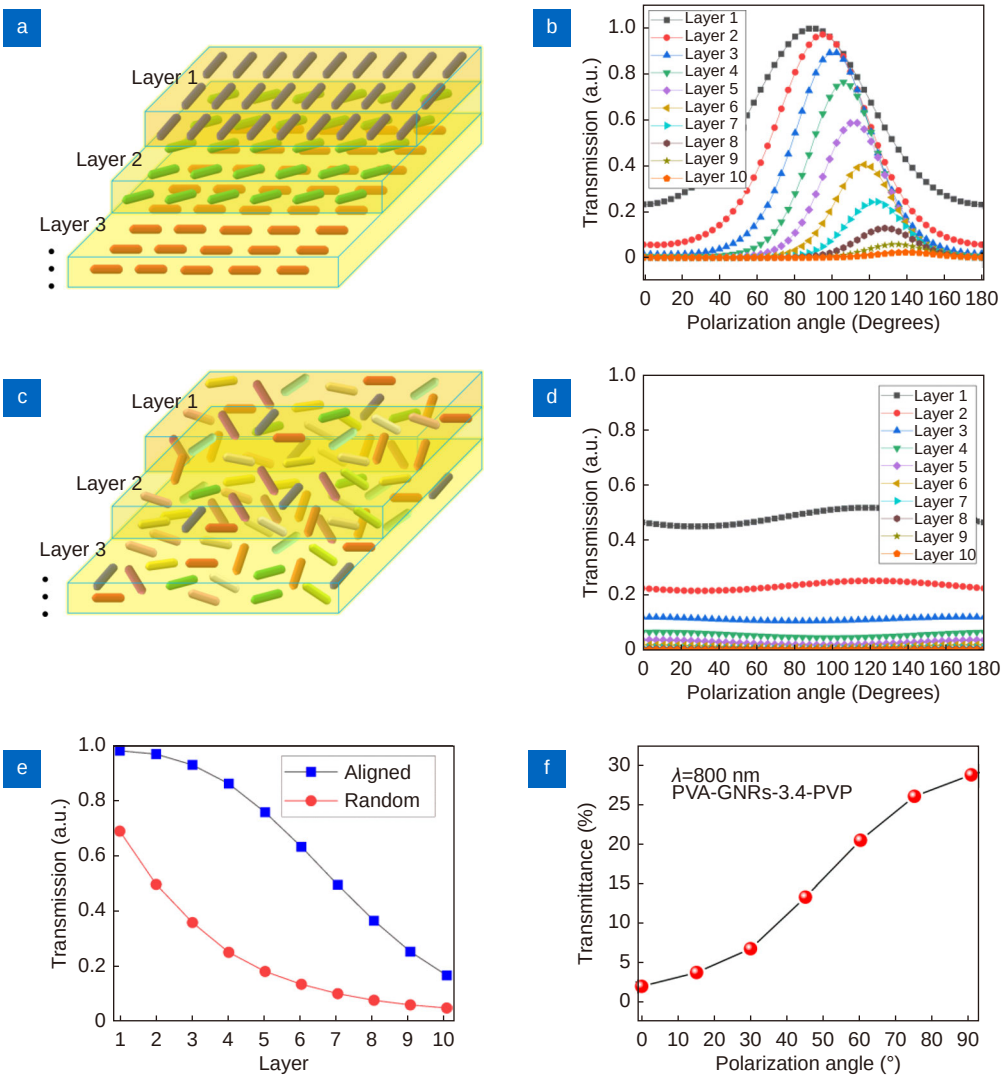

Fig. S7 | (**a**) Schematic drawing of the GNRs with single size and aligned in the same direction, slightly twisted angle from progressively from the first layer to the last layer. (**b**) Polarization-dependent transmission through 10 layers with aligned GNRs. (**c**) Schematic drawing of the multilayered ODS medium with randomly aligned GNRs. (b) Polarization-dependent transmission through 10 layers with randomly aligned GNRs. (**e**) Comparison of transmission between the aligned and randomly aligned GNRs throughout the layers. (**f**) The transmittance as a function of the polarization angle measured the sample (PVA-GNRs-3.4-PVP) at the wavelength of 800nm in the experiment.

References

1. Ye XC, Gao YZ, Chen J, Reifsnyder DC, Zheng C, et al. Seeded growth of monodisperse gold nanorods using bromide-free surfactant mixtures. *Nano Lett* **13**, 2163–2171 (2013).
2. Nikoobakht B, El-Sayed MA. Preparation and growth mechanism of gold nanorods (NRs) using seed-mediated growth method. *Chem Mater* **15**, 1957–1962 (2003).
3. Li XP, Lan TH, Tien CH, Gu M. Three-dimensional orientation-unlimited polarization encryption by a single optically configured vectorial beam. *Nat Commun* **3**, 998 (2012).
4. Taylor AB, Michaux P, Mohsin AS, Chon JW. Electron-beam lithography of plasmonic nanorod arrays for multilayered optical storage. *Opt Express* **22**, 13234–13243 (2014).
5. Taylor AB, Chon JWM. Angular photothermal depletion of randomly oriented gold nanorods for polarization-controlled multilayered optical storage. *Adv Opt Mater* **3**, 695–703 (2015).